Sedimentation and Diffusion in Suspensions of Sterically Stabilized Colloidal Platelets

ARTICLE *in* LANGMUIR · MAY 2000

Impact Factor: 4.46 · DOI: 10.1021/la991571b

3 AUTHORS, INCLUDING:

Albert P Philipse
Utrecht University
189 PUBLICATIONS **6,443** CITATIONS

SEE PROFILE

Sedimentation and Diffusion in Suspensions of Sterically Stabilized Colloidal Platelets

F. M. van der Kooij,[†] A. P. Philipse,*[,†] and J. K. G. Dhont[‡]

Van't Hoff Laboratory for Physical and Colloid Chemistry, Debye Institute, Utrecht University, Padualaan 8, 3584 CH Utrecht, The Netherlands, and Forschungszentrum Jülich, IFF Weiche Materie, D-52425 Jülich, Germany

Received December 1, 1999. In Final Form: March 6, 2000

Ultracentrifuge and light scattering measurements are performed to study static and dynamic properties for a suspension of well-defined platelike colloids to first order in concentration. Both the form factor and the diffusion coefficient at infinite dilution match theoretical expressions if polydispersity is incorporated. This yields values for the polydispersity corresponding with values obtained from electron microscopy. Application of the generalized Stokes−Einstein relation to the measured concentration dependence of sedimentation and collective diffusion coefficients yields a second virial coefficient B_2 for the platelets which is slightly smaller than the theoretical value for hard disks.

1. Introduction

In industrial applications, colloids are frequently used as thickeners, fillers, and antisettling agents. These applications often concern colloidal clay platelets, which combine distinct transport properties with abundant availability. The physical properties of suspensions of clay platelets have therefore been addressed in many studies. Typical properties such as complex interactions, flexibility, and polydispersity make clays however less suitable as a simple model system for platelike particles. Instead, the study of the relation between platelike particle shape and physical suspension properties requires a model system of well-defined, hard (e.g., short-range repulsive) platelike particles. For instance the aforementioned complex interactions cause suspensions of clay platelets to gel,[1,2] in contrast with the formation of liquid crystals which is predicted for *hard* plates by computer simulations.[3,4] Recently we reported on a model system of sterically stabilized colloidal gibbsite ($Al(OH)_3$) platelets in toluene,[5] which does show the predicted nematic liquid crystalline phase. Here we adopt this well-defined system for (nearly) hard plates to focus on the various properties which can be measured by sedimentation measurements and static and dynamic light scattering. For hard plates, experimental data on such properties are lacking. For free platelets the friction factor[6] and light scattering form factor[7] have been calculated. The concentration dependence of sedimentation and diffusion, on the other hand, has been calculated for spheres[8,9] and for rods[10,11] but not for platelets. In this study we will consider two suspensions of the aforementioned model system for hard plates, which differ by the average aspect ratios of the constituent platelets (6.5 and 12, respectively). This allows us to investigate the influence of particle shape and anisometry on the form factor and the volume fraction dependence of diffusion and sedimentation. Using polydispersity as the fitting parameter, we will compare the measured light scattering and sedimentation properties at infinite dilution to theoretical expressions. Values for the polydispersity obtained this way will be compared to those obtained from electron microscopy. The generalized Stokes−Einstein relation will be applied to relate the measured concentration dependence of sedimentation and collective diffusion to the second virial coefficient of the plates.

2. Theoretical Background

2.1. Sedimentation. The sedimentation coefficient s of a suspended particle is defined as the sedimentation velocity normalized by the gravitational or the centrifugal acceleration. At infinite dilution[12]

$$s_0 = (m_p - m_0)/f_0 = V_p(\rho_p - \rho_0)/f_0 \qquad (1)$$

Here $m_p - m_0$ denotes the mass of the particle minus that of the solvent displaced by the particle, and ρ_p, ρ_0 are the mass densities of the particle and the solvent, respectively. The translational friction factor at infinite dilution f_0 is the Stokes friction for a particle in a solvent with viscosity η_0. The anisometry of platelike particles gives rise to different friction factors for translations either parallel ($f_{||}$) or perpendicular ($f_\perp$) to their orientation, that is, to the plate normal. For oblate spheroids, modeling disk-shaped particles, theoretical expressions for $f_{||}$ and $f_\perp$ in the limit of infinite dilution were derived by Brenner.[6] For high aspect ratios d/l, with d being the diameter and l the thickness of the plates, the expressions reduce to

$$f_{||} = 8\eta_0 d \quad \text{and} \quad f_\perp = \frac{16}{3}\eta_0 d, \qquad \text{for } \frac{d}{l} \to \infty \qquad (2)$$

Analogous to the case of rods,[13] the effective friction factor f_{eff} of randomly oriented plates is found as the following average:

[†] Utrecht University.
[‡] Forschungszentrum Jülich.

(1) Mourchid, A.; Delville, A.; Lambard, J.; Lecolier, E.; Levitz, P. *Langmuir* **1995**, *11*, 1942.
(2) Gabriel, J.; Sanchez, C.; Davidson, P. *J. Phys. Chem.* **1996**, *100*, 11139.
(3) Eppenga, R.; Frenkel, D. *Mol. Phys.* **1984**, *52*, 1303.
(4) Veerman, J.; Frenkel, D. *Phys. Rev. A* **1992**, *45*, 5632.
(5) van der Kooij, F.; Lekkerkerker, H. *J. Phys. Chem. B* **1998**, *102*, 7829.
(6) Brenner, H. *J. Multiphase Flow* **1974**, *1*, 195.
(7) Guinier, A.; Fournet, G. *Small Angle Scattering of X-rays*; John Wiley and Sons: New York, 1955.
(8) Batchelor, G.; Green, J. T. *J. Fluid Mech.* **1972**, *56*, 401.
(9) Batchelor, G. *J. Fluid Mech.* **1976**, *74*, 1.
(10) Dogic, Z.; Fraden, S.; Dhont, J. Manuscript in preparation.
(11) Szamel, G. *Phys. Rev. Lett.* **1993**, *70*, 3744.
(12) Svedberg, T.; Pedersen, K. O. *The Ultracentrifuge*; Theodor Steinkopff: Dresden, Germany, 1940.

10.1021/la991571b CCC: $19.00
Published on Web 05/11/2000

$$\frac{1}{f_{\text{eff}}} = \frac{1}{3}\left(\frac{1}{f_{\parallel}} + \frac{2}{f_{\perp}}\right) = \frac{1}{6\eta_0 d}, \quad \text{for } \frac{d}{l} \to \infty \tag{3}$$

Hence the effective friction coefficient of an infinitely thin oblate ellipsoid equals $2/\pi$ of that of a sphere with equal diameter.

In dilute suspensions, the normalized sedimentation coefficient of particles without long-range double-layer interactions is in general linearly dependent on the volume fraction

$$\frac{s(\phi)}{s_0} = 1 + K_2\phi \tag{4}$$

Hence K_2, which equals -6.55 for hard spheres,[8] reflects the volume fraction dependence of the collective friction. Attractive particle interactions make the value of K_2 less negative[14] or even positive because the resulting decrease in particle separations reduces the effect of back-flow, while back-flow is the main contribution to K_2. For platelike particles the value of K_2 has neither been measured nor calculated. Qualitatively, one would expect the value of K_2 to become more negative as the degree of anisometry increases, since the resulting increase in excluded volume enhances their exposure to back-flow.

2.2. Light Scattering. *2.2.1. Static Light Scattering.* In static light scattering the time average of the scattered light is measured, for which the Rayleigh ratio R in the case of *spherical* particles can be expressed as

$$R(K) = AcMP(K)\,S(K) \propto V_p^{\,2}\,P(K)\,S(K) \tag{5}$$

where A is a constant containing optical factors, c the weight concentration, M the molar mass, and V_p the volume of the particles. Furthermore, $P(K)$ represents the form factor of the particles and $S(K)$ the static structure factor of the suspension. The scattering wave vector K is defined as

$$K = (4\pi n/\lambda)\sin(\theta/2) \tag{6}$$

with n being the refractive index of the medium, λ the wavelength of the incident light in vacuo, and θ the scattering angle. For nonspherical, interacting particles the K-dependence in eq 5 cannot be factorized into $P(K)$ $S(K)$ because of the correlation between orientation and position in this case. Therefore eq 5 only applies to suspensions of plates at very low concentrations, where $S(K) = 1$, or for very small K such that $P(K) = 1$. The orientationally averaged form factor for a cylinder of revolution (e.g., a disk) with diameter d and thickness l is given by[7]

$$P(K) = \int_0^{\pi/2} \frac{\sin^2(K(l/2)\cos\theta)}{(K(l/2)\cos\theta)^2} \frac{4J_1^{\,2}(K(d/2)\sin\theta)}{(K(d/2)\sin\theta)^2} \sin\theta\,\mathrm{d}\theta \tag{7}$$

with J_1 being the first order Bessel function and θ the angle between the plate normal and the incident beam. The form factor of an assembly of polydisperse disks is obtained by integrating over $P(K)$ of all constituent particles,[15] which includes a $V_p^{\,2}$ proportionality to account for the scattering power of the species (eq 5)

$$P^{\text{pol}}(K) = \frac{\int_0^\infty\int_0^\infty V_p^{\,2}F(d,l)\,P(K,d,l)\,\mathrm{d}d\,\mathrm{d}l}{\int_0^\infty\int_0^\infty V_p^{\,2}F(d,l)\,\mathrm{d}d\,\mathrm{d}l} \tag{8}$$

with $F(d,l)$ being the probability density function for the particle diameter and thickness.

2.2.2. Dynamic Light Scattering. Dynamic light scattering probes the intensity fluctuations of the scattered light, which are characterized by the normalized intensity autocorrelation function. This so-called IACF is related to the EACF, the normalized electric field autocorrelation function, by means of the Siegert relation:

$$\hat{g}_I(K,t) = 1 + |\hat{g}_E(K,t)|^2 \tag{9}$$

While for spheres the decay of the autocorrelation functions in time is solely due to translational Brownian motion, there is an additional contribution by rotational Brownian motion in the case of anisometric particles. Analogous to the case of rods,[15] the EACF for very dilute suspensions of plates can for short times be written as

$$\hat{g}_E(K,t) = \exp(-[C(K,d,l)\Delta D + D_0]K^2t)[S_0(K,d,l) + S_2(K,d,l)\exp(-6D_{0,r}t) + S_4(K,d,l)\exp(-20D_{0,r}t) + \ldots] \tag{10}$$

where the function $C(K,d,l)$ expresses the coupling between translation and rotation, which arises from the connection between translational diffusivity and orientation of a plate. Further, $\Delta D = D_{0,\perp} - D_{0,\parallel}$ is the difference between the perpendicular and parallel translational diffusion coefficients at infinite dilution, and D_0, $D_{0,r}$ represent the orientationally averaged translational and rotational diffusion coefficients at infinite dilution, respectively. Numerical results for $C(K,d,l)$ and the $S_{2n}(K,d,l)$ coefficients for plates are given in Appendix B, showing that translation−rotation coupling and the S_{2n}, $n > 0$, terms can be neglected for $Kd < 5$. The IACF then reduces to

$$\hat{g}_I(K,t) = 1 + \exp(-2D_0K^2t), \quad \text{for } Kd < 5 \tag{11}$$

While for monodisperse particles D_0 is K−independent, the apparent D_0 which is measured for a polydisperse system is K−dependent and equal to[15]

$$D_0^{\text{pol}}(K) = \frac{\int_0^\infty\int_0^\infty V_p^{\,2}F(d,l)P(K,d,l)\,D_0(d,l)\,\mathrm{d}d\,\mathrm{d}l}{\int_0^\infty\int_0^\infty V_p^{\,2}F(d,l)P(K,d,l)\,\mathrm{d}d\,\mathrm{d}l} \tag{12}$$

In the evaluation of eq 12 we use the relation $D_0(d,l) = kT/f_0(d,l)$; for $f_0(d,l)$ we will use a fit of the full expression for the d and l dependence of the theoretical friction factor for orientationally averaged plates.[6]

2.3. Generalized Stokes−Einstein Relation. The concentration dependence of collective diffusion D_c and sedimentation are related according to the generalized Stokes−Einstein relation[16]

(13) de Keizer, A.; van der Drift, W.; Overbeek, J. *Biophys. Chem.* **1975**, *3*, 107.
(14) Jansen, J.; de Kruif, C.; Vrij, A. *J. Colloid Interface Sci.* **1986**, *114*, 501.
(15) Dhont, J. *An Introduction to the Dynamics of Colloids*; Elsevier: Amsterdam, 1996.
(16) Pusey, P. *Dynamic Light Scattering: Applications of Photon Correlation Spectroscopy*; Plenum: New York, 1985.

$$\frac{D_c(\phi,K=0)}{D_0} = \frac{s(\phi)}{s_0}\frac{1}{kT}\left(\frac{\partial\Pi}{\partial\rho}\right)_T \quad (13)$$

where D_0 denotes the diffusion coefficient at infinite dilution, and $\partial\Pi/\partial\rho$ the inverse of the systems' osmotic compressibility with ρ being the number density. Using the expression for the volume fraction dependence of the sedimentation coefficient (eq 4) and a similar $\phi-$expansion for collective diffusion

$$D_c(\phi,K=0)/D_0 = 1 + \alpha\phi + ... \quad (14)$$

and the osmotic compressibility,

$$\frac{1}{kT}\frac{\partial\Pi}{\partial\rho} = 1 + 2B_2\rho + ... = 1 + 2B_2{}^*\phi + ... \quad (15)$$

where $B_2{}^* = B_2/v_0$, the second virial coefficient normalized by the particle volume, we find from the generalized Stokes−Einstein relation that

$$\alpha = 2B_2{}^* + K_2 \quad (16)$$

For hard spheres, the first order $\phi-$coefficient for collective diffusion α then becomes

$$\alpha = 8 - 6.55 = 1.45 \quad (17)$$

while for randomly oriented hard disks

$$\alpha = \frac{\pi}{2}\frac{d}{l} + 3 + \pi + 2\frac{l}{d} + K_2 \quad (18)$$

where it was used that for randomly oriented particles $B_2 = v_{ex}/2$, with v_{ex} being the excluded volume of two disks.[17]

3. Experimental Section

3.1. Model System of Platelike Colloids. The model system of sterically stabilized platelets examined in this study consists of gibbsite ($Al(OH)_3$) platelets, which are grafted with a polyisobutene layer. The synthesis of the aqueous suspension of gibbsite[5,18−20] was adapted such that two suspensions of platelets with different aspect ratios were obtained. This variation was achieved by choosing the HCl concentration in the starting (0.08 M aluminium−*sec*-butoxide + 0.08 M aluminium−isopropoxide) solutions to be either 0.09 or 0.04 M. These solutions were autoclaved for 72 h at 85 °C. The suspensions were subsequently grafted with a polyamine modified polyisobutene ($M_w = 1000$), which was provided by Shell Research Ltd., after which they were coded A10P and A11P, respectively. The thickness of the polymer layer is approximately 4 nm.[21] Transmission electron microscope (TEM) micrographs are shown in Figure 1. The distributions of plate diameters, as determined from TEM micrographs by measuring the diameter of a circle with an area equal to that of a particle, are depicted in Figure 2. The corresponding number average and relative standard deviation $[\langle d\rangle^2 - \langle d^2\rangle]^{1/2}/\langle d\rangle$, as well as the aspect ratio of the particles, are given in Table 1. Note that the given aspect ratio reflects the grafted particle, as determined from the intrinsic viscosity.[22] Alternatively, the aspect ratio may be established indirectly from the TEM diameter and thickness, by adding the estimated thickness of the polymer layer. Determination of the thickness by TEM was only possible after deliberately flocculating the samples because stable platelets are virtually always oriented flat on the TEM grid surface. The resulting aspect ratio of the grafted platelets is 13 for A10P and 8 for A11P. Alternatively, we determined the thickness by X-ray diffraction using Scherrer's equation for the broadening of the (002) peak. This gives aspect ratios of 10 and 5 for A10P and A11P, respectively. Volume

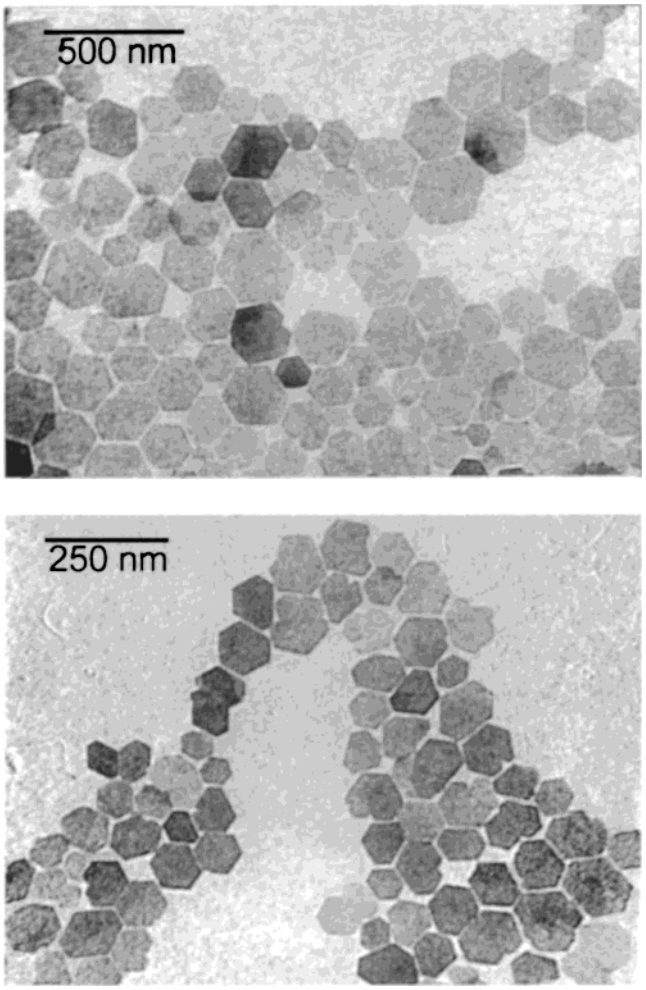

Figure 1. Transmission electron microscope (TEM) micrograph of (top) A10P and (bottom) A11P suspensions.

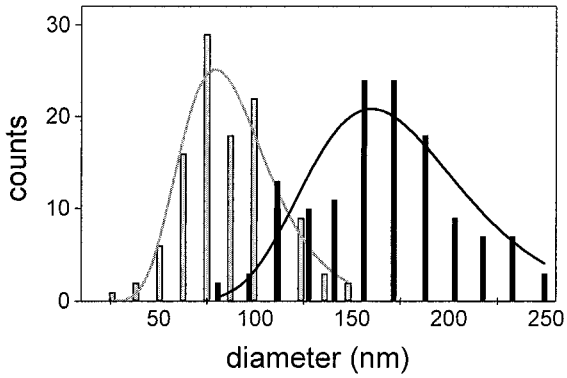

Figure 2. Diameter distributions as measured for the A10P (black) and A11P (grey) systems by TEM. The drawn lines are log-normal fits of the measured distributions.

Table 1. Results of Particle Characterization

syst code	core diam (nm)	aspect ratio[a]
A10P	165 (±25%)	12
A11P	85 (±30%)	6.5

[a] The aspect ratio of the grafted particles as determined from their intrinsic viscosity.[22]

(17) Onsager, L. *Ann. N. Y. Acad. Sci.* **1949**, *51*, 627.
(18) Buining, P.; Pathmamanoharan, C.; Jansen, J.; Lekkerkerker, H. *J. Am. Ceram. Soc.* **1991**, *74*, 1303.
(19) Philipse, A.; Nechifor, A.; Patmamanoharan, C. *Langmuir* **1994**, *10*, 4451.
(20) Wierenga, A.; Lenstra, T.; Philipse, A. P. *Colloids Surf. A* **1998**, *134*, 359.
(21) Smits, C.; Briels, W.; Dhont, J.; Lekkerkerker, H. *Prog. Colloid Polym. Sci.* **1989**, *79*, 287.
(22) van der Kooij, F.; Boek, E.; Philipse, A. Manuscript in preparation.

fractions were calculated as the solid mass content of samples, divided by the effective particle density ρ_{eff} which includes the solvent immobilized in the grafted polymer layer.[22,23] The value of ρ_{eff} was determined as 1.3 and 1.1 g/cm^3 for the A10P and A11P particles, respectively, each with an estimated error of 10% due to the uncertainty in the polymer layer thickness.

3.2. Sedimentation Measurements. Sedimentation measurements were performed with a Beckman Optima XL-A analytical ultracentrifuge equipped with scanning absorption optics. Measurements were performed at 25 ± 0.1 °C. The absorption peak of the grafted polymer layer on the platelets at $\lambda = 405$ nm was used as the detection wavelength. The radial step size of the scans was 50 μm. With this setup sedimentation profiles could be measured accurately for dispersions of volume fractions down to about 0.5% (v/v). To minimize boundary spreading by diffusion, rotor speeds of 4500 and 6000 rpm were selected for the A10P and A11P dispersions, respectively. The movement of the sedimentation boundary was analyzed using the second moment method.[24] Sedimentation coefficients were calculated as the average of three measurements, each based on a time series of nine scans.

3.3. Light Scattering Experiments. Dynamic light scattering (DLS) measurements were carried out in *VV* polarization mode using a Spectra Philips model 2020 krypton laser at 647.1 nm wavelength. Normalized intensity autocorrelation functions were collected with a Malvern 7032 CE 128-channel correlator. For the given diameter of the platelets and the *K*-vectors for which DLS measurements were performed, *Kd* in these experiments never exceeds the value of 4. Short-time diffusion coefficients were obtained from the slope of ln $\hat{g}_1(K,t)$ vs K^2t (see eq 11). The required base-line parameter β was obtained from a single exponential fit of the full IACF. Measurements were performed at 25 ± 0.1 °C on samples ranging in volume fraction from about 5×10^{-4} to 5×10^{-2}. Samples were made dust-free by filtration through a 1.2 μm Millipore filter.

4. Results and Discussion

4.1. Sedimentation. As a result of the polydispersity of the suspensions, significant boundary spreading during sedimentation is observed for the more dilute samples. Upon increasing the concentration, boundary spreading is opposed by self-sharpening of the boundary due to the concentration dependence of the sedimentation velocity. In Appendix A it is discussed to what extent the apparent weight average sedimentation coefficient obtained in a sedimentation experiment is affected by polydispersity. A striking characteristic of the radial sedimentation absorbance profiles is the appearance of a peak in the absorbance, as depicted in Figure 3. The position of the peak is always close to the boundary and appears only if the sample volume fractions exceed 0.03 (A10P) or 0.04 (A11P). Recently,[10] the presence of an apparently similar peak has been explained as an artifact of the apparatus which originates from the refraction of the incident light at the sharp sedimentation boundary. Nevertheless, the peak in the absorbance does not obstruct unambiguous determination of the sedimentation velocity. The reason for this is that the employed second moment method determines the movement of area under the absorbance curve, while the area associated with the peak is relatively small and is characterized by almost the same sedimentation coefficient as the bulk.

Results of the sedimentation measurements are depicted in Figure 4. The error bars shown are based on the spreading of three separate measurements, while the error in K_2, the slope of s/s_0 vs ϕ, also takes into account the uncertainty in the volume fraction. We find that $K_2 = -10.9 \pm 1.1$ and -5.8 ± 0.6 for the A10P and A11P systems,

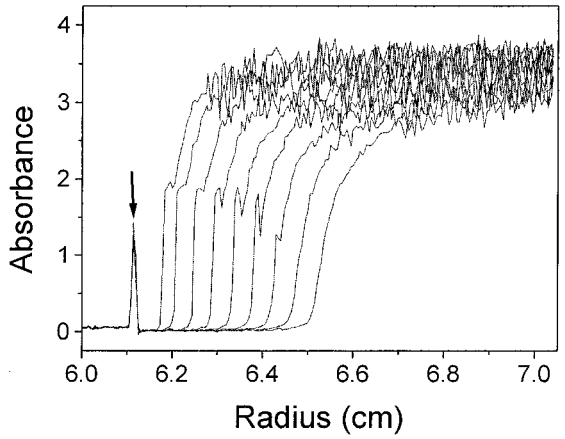

Figure 3. Radial sedimentation absorbance profiles plotted as a function of sedimentation time. Shown here is the scan series for the A10P suspension at $\phi = 0.033$, which is typical for the sedimentation behavior of the suspensions at higher concentrations. The arrow marks the position of the solvent meniscus. The noise in the upper plateau for this sample is probably caused by the vicinity of the maximum detection limit of the apparatus.

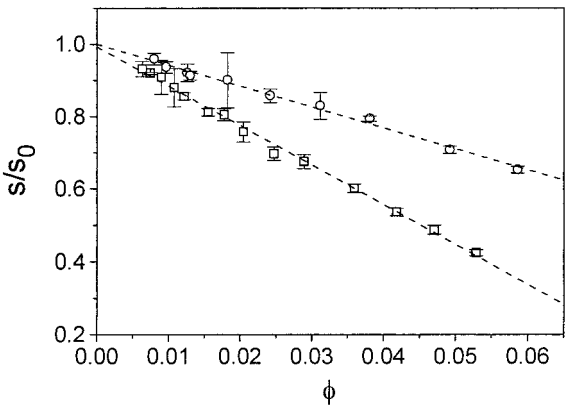

Figure 4. Normalized sedimentation coefficients as a function of the volume fraction. For the A10P dispersion (□) $s_0 = (2.32 \pm 0.01) \times 10^{-10}$ s, while for the A11P suspension (○) $s_0 = (1.31 \pm 0.01) \times 10^{-10}$ s. The dashed lines are linear fits to the measured data with a slope equal to K_2.

respectively. As expected qualitatively from the influence of the excluded volume of the particles, a marked difference in K_2 is observed between these systems following from their disparity in anisometry. The value of K_2 for the A11P system of low anisometry is close to the value for hard spheres.

4.2. Form Factor for Polydisperse Plates. In the previous section we mentioned that the determination of the sedimentation coefficient is only slightly complicated by the system's polydispersity. Light scattering on the other hand is much more sensitive to polydispersity because the scattered intensity is proportional to the squared particle volume (eq 8). The influence of polydispersity is most notably present in the limit $K \rightarrow 0$, where the contribution of the strongly scattering larger particles is most pronounced. As shown in Figure 5, the *K*-dependence of the light scattered by very dilute suspensions reflecting the experimental form factor can be fitted by evaluating eq 8 for a particular diameter distribution. It should be noted that agreement with the experimental scattering profile can be obtained for more than one particle diameter/polydispersity combination. Here polydispersity was used as the fitting parameter while leaving the average particle diameter fixed at the average diameter of the gibbsite core obtained by electron mi-

(23) van Bruggen, M.; Dhont, J.; Lekkerkerker, H. *Macromolecules* **1999**, *32*, 2256.
(24) Goldberg, R. *J. Phys. Chem.* **1953**, *57*, 194.

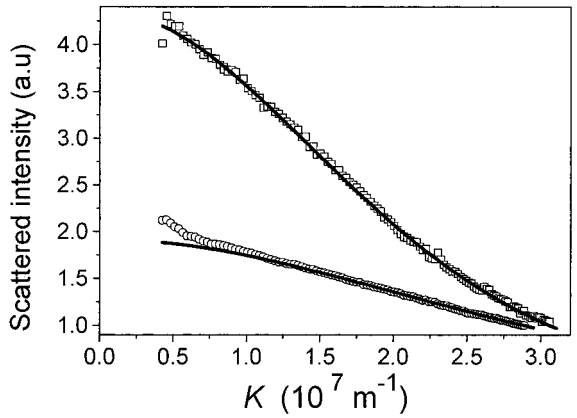

Figure 5. Static light scattering profiles for very dilute suspensions: (□) A10P at $\phi = 8 \times 10^{-4}$ and (○) A11P at $\phi = 2 \times 10^{-3}$. The intensity data are arbitrarily normalized at the value at high K. Drawn lines represent the fits through the experimental data following eq 8 for a given diameter and polydispersity.

Table 2. Results of Fitting the Static and Dynamic Light Scattering Data

	SLS	DLS	
syst code	polydispersity (%)	f_0/f_0^{th} [a]	polydispersity (%)
A10P	27 ± 2	1.00 ± 0.02	39 ± 3
A11P	35 ± 2	1.09± 0.02	53 ± 5

[a] The ratio of the friction factor used in the evaluation of eq 12 and the theoretical friction factor[6] for randomly oriented oblate spheroids with a particular diameter and thickness. Error margins are given to indicate the tolerance for agreement between a calculated fit and the experimental data.

croscopy. For the probability density function $F(d)$ in eq 8 we adopted a log-normal distribution, which seems the best representation of the diameter distribution function determined from TEM images (Figure 2). Furthermore, we only consider polydispersity in diameter, neglecting any (experimentally undetermined) polydispersity in the thickness of the plates. The form factor is however practically independent of (variations in) thickness since $Kl \ll 1$. The agreement between the experimental and calculated scattering profile is very sensitive for the chosen polydispersity. The best fit is obtained for values of the polydispersity (Table 2) which strongly resemble the standard deviation obtained from TEM images (Table 1). A small deviation of the experimental scattering from the calculated curve is observed for the A11P suspension in the small-K regime. This suggests that this sample contains a minor amount of relatively large contaminating scattering entities, which may contribute significantly to the small K scattering because of the low sample concentration and the poor scattering power of the small A11P platelets.

4.3. Collective Diffusion. For a range of K-vectors, measured diffusion coefficients as a function of the platelet volume fraction are plotted in Figure 6. In accordance with the polydisperse nature of the model system used, D_0, which follows from Figure 6 by extrapolating to $\phi = 0$, shows a marked dependence on K. This K-dependence is accounted for in eq 12, as shown in Figure 7. The calculated curve is based on two independent fitting parameters, the friction factor and the polydispersity. The friction factor f_0 affects the calculated diffusion coefficient according to $D_0(K) \propto f_0^{-1}$ for all K, while the polydispersity determines the curvature of D_0 vs K. Fitting therefore yields a single solution for the friction factor and polydispersity, which is shown in Table 2. The polydispersity

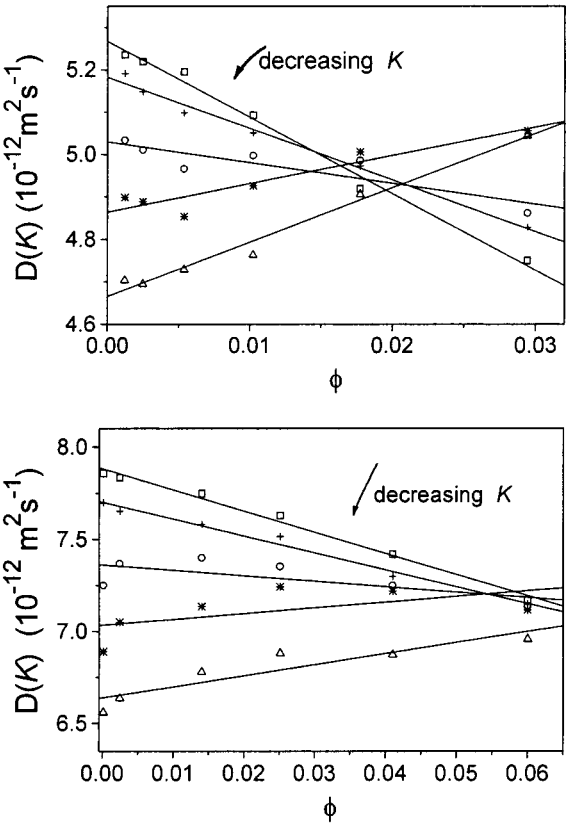

Figure 6. Diffusion coefficients as a function of the volume fraction, measured for several scattering wave vectors K: (top) A10P suspension for $K =$ (△) 1.27×10^7, (*) 1.64×10^7, (○) 1.98×10^7, (+) 2.27×10^7, and (□) 2.51×10^7 m^{-1}; (bottom) A11P suspension for $K =$ (△) 1.09×10^7, (*) 1.52×10^7, (○) 1.90×10^7, (+) 2.24×10^7, and (□) 2.51×10^7 m^{-1}.

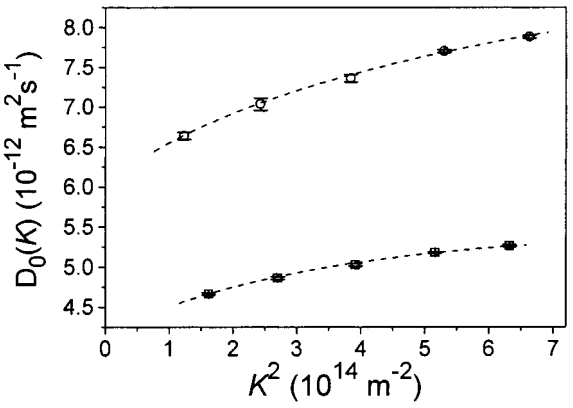

Figure 7. Diffusion coefficient at infinite dilution, as obtained by extrapolation of the linear fits in Figure 6 to $\phi = 0$, as a function of the squared wave vector: (□) A10P and (○) A11P. Dashed lines represent fits of the data according to eq 12.

obtained this way is somewhat higher than values based on electron micrographs and static light scattering. Excellent agreement is observed between the friction factor and theoretical values for randomly oriented oblates.[6] As in the evaluation of $P^{pol}(K)$, only the polydispersity in platelet diameter was taken into account in the calculation of $D_0^{pol}(K)$. This seems justified by the fact that (variations in) plate thickness hardly affects $D_0(K)$ in the present case, where $Kl \ll 1$, since the dependence of both $P(K)$ and D_0 [6] on the platelet thickness is rather weak. Note that in the evaluation of $D_0^{pol}(K)$ (eq 12) the dimensions of the scattering entity refer to that of the gibbsite core, whereas the hydrodynamic particle volume, which includes the

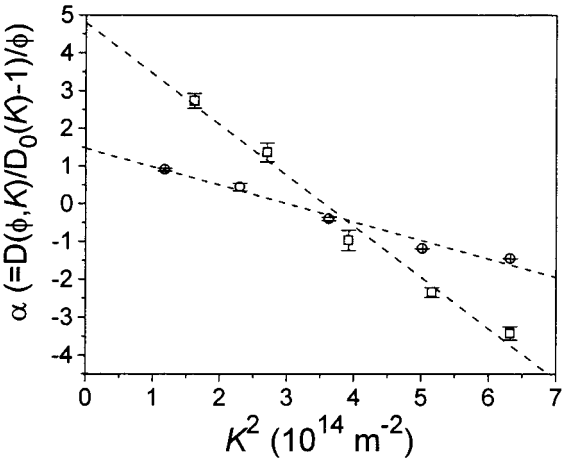

Figure 8. The first order ϕ−coefficient for diffusion (α), extrapolated to $K = 0$ according to K^2 to obtain the volume fraction dependence of collective diffusion (eq 14).

Table 3. Experimental and Theoretical Second Virial Coefficients

			B_2*	
syst code	$\alpha(K \rightarrow 0)$	K_2	expt	hard disk[17]
A10P	4.8 ± 0.6	−10.9 ± 1.1	7.9 ± 0.6	12.5
A11P	1.5 ± 0.3	−5.8 ± 0.6	3.7 ± 0.3	8.3

grafted polymer layer, appears in the expressions related to the friction of the particles.

As shown in Figure 6 for the K-vectors studied, the volume fraction dependence of the measured short-time diffusion is linear. The slope of this fit, divided by the value of $D(K)$ at $\phi = 0$, yields the K-dependent first order ϕ−coefficient for diffusion $\alpha(K)$. Since the hydrodynamic function and the structure factor underlying eq 13 are both even functions of K, $\alpha(K)$ is extrapolated to $K = 0$ from a plot against K^2 (Figure 8). The resulting second virial coefficients, as calculated from the measured $\alpha(K=0)$ and K_2 coefficients, are slightly to moderately lower than theoretical values for hard disks (Table 3). This may be indicative for a trace of van der Waals attraction between the platelets; however the nature of the underlying experiments does not allow quantitative judgment in this respect.

In principle, another way to determine second virial coefficients is to measure the structure factor from the scattered intensity (eq 5). However in the case of the anisometric particles studied here, it is not allowed to extract the structure factor from the scattering profile because of the unfactorizability of the form and structure factors. Furthermore, our experimental setup does not give absolute values for scattered intensity, and the accessible K-range does not allow normalizing $S(K) = 1$ at high K.

4.4. Particle Mass. From the Svedberg equation (eq 1) it follows that the particle mass can be calculated from the product of the sedimentation and friction coefficient at infinite dilution. In the present case, the volume of the grafted polymer is unknown but its density is almost equal to that of the solvent, and therefore eq 1 may also be written as

$$s_0 f_0 = V_{core}(\rho_{core} - \rho_0) + V_{pol}(\rho_{pol} - \rho_0) \approx m_{core}(1 - \rho_0/\rho_{core}) \quad (19)$$

with ρ_{core} being the mass density of gibbsite (2.42 g cm^{-3})[25] and ρ_0 the density of toluene. The resulting mass of the gibbsite core is related to its dimensions according to

$$m_{core} = \frac{\pi}{4}(d^2 l)_{core}\rho_{core} \quad (20)$$

with d being the (circle-equivalent) TEM diameter and l the thickness of the plates. Here we will fix the core diameter to determine the thickness of the core, as the core diameter is well-established by TEM. The core thickness cannot be determined unambiguously by TEM because the orientation of the platelets on the TEM grid does not allow (exactly perpendicular) edgewise imaging. The thickness resulting from s_0 is shown in Table 4. Although these results are probably the most reliable data available for the core thickness, we do not employ them to calculate the aspect ratio of the grafted platelets as the polymer thickness is less well-defined, and the aspect ratio of the grafted particles is accessible directly from the intrinsic viscosity.

Table 4. Determination of Particle Mass from the Combined Sedimentation and DLS Results

syst code	f_0[a] (10^{-10} kg s^{-1})	s_0[b] (10^{-10} s)	m_{core}[c] (10^{-19} kg)	l_{core}[d] (nm)
A10P	5.7 ± 0.1	2.06 ± 0.01	1.8 ± 0.1	3.5
A11P	3.4 ± 0.1	1.11 ± 0.10	0.59 ± 0.02	4.3

[a] Friction coefficient at infinite dilution according to Table 2, based on the number-average aspect ratio. [b] Number-average sedimentation coefficient at infinite dilution, calculated from the experimental s_0 (Figure 4) using eq 22. [c] Number-average mass of the gibbsite core following from the combined sedimentation and friction coefficient, according to eq 19. [d] Calculated number-average thickness l of the gibbsite core, using its number-average TEM diameter and eq 20.

5. Conclusions

Using a well-defined model system, we have studied various sedimentation and light scattering properties for (nearly) hard plates. Comparison of the measured translational friction factor at infinite dilution and the form factor with theoretical predictions yields values for the system's polydispersity which resemble those obtained from electron microscopy. The second virial coefficient of the platelets, which can be calculated from the measured volume fraction dependence of collective diffusion and sedimentation coefficients by applying the generalized Stokes−Einstein relation, suggests that the particles can be considered as fairly hard disks. Our results clearly show the need for theoretical and computational efforts regarding platelike particles, particularly with respect to the first order ϕ−coefficient for sedimentation and diffusion.

Appendix A: Sedimentation of Polydisperse Particles

In a sedimentation experiment using an analytical ultracentrifuge equipped with absorbance scanning optics, weight-average sedimentation coefficients are measured because each particle species i of a polydisperse system contributes to the signal proportional to the mass (or volume) of that species, so for the value at infinite dilution one finds

$$s_0^{exp} = \sum_i n_i V_{p,i} s_{0,i}(d) / \sum_i n_i V_{p,i} \quad (21)$$

(25) Gitzen, W. Alumina as a Ceramic Material; The American Ceramic Society: Columbus, OH 1970.

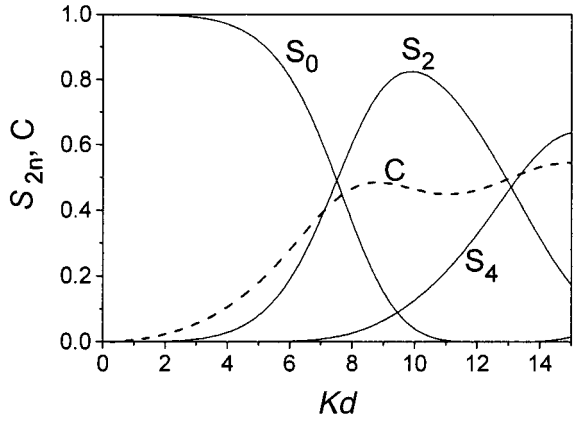

Figure 9. Calculated coefficients reflecting the contributions of translational and rotational diffusion to the decay of the intensity autocorrelation function for disks. For $Kd < 5$, the S_{2n} ($n > 0$) coefficients describing the weight of rotational contributions is subordinate to the $n = 0$ coefficient reflecting purely translational diffusion. The rotation−translation coupling function $C(Kd)$ is also small in this regime.

Using eqs 1−3, this can be written as

$$s_0^{\text{exp}} \approx \text{constant}\langle d_i^3\rangle\langle l\rangle/\langle d_i^2\rangle\langle l\rangle \approx \text{constant}(1 + 2\sigma^2)\langle d\rangle \tag{22}$$

where it was assumed that the diameter d and thickness l of the platelets are uncorrelated. Such lack of correlation seems plausible since TEM images do not show a connection between the diameter of a particle and its contrast on TEM, the latter being indicative for the plate thickness. Hence the measured sedimentation coefficient is approximately $(1 + 2\sigma^2)$ times larger than the number-averaged sedimentation coefficient, which is a factor of 1.13 and 1.18 in case of the A10P and A11P particles, respectively.

Appendix B: Contribution of Rotational Diffusion to the EACF for Plates

In analogy with the case of rods[15] the electric field autocorrelation function (EACF) of very dilute isotropic suspensions of plates can, if the relative difference $\Delta\epsilon/\bar{\epsilon}$ in the dielectric constants parallel and perpendicular to the plate normal is small, be written as

$$\hat{g}_E(K,t) = \frac{\langle j(d,l,K\hat{u}(t_0))\, j(d,l,K\hat{u}(t)\exp[iKr(t_0) - r(t)])\rangle}{\langle j^2(d,l,K\hat{u})\rangle} \tag{23}$$

where $\langle j^2(d,l,K\hat{u})\rangle$ is the orientational-averaged form factor $P(K)$ of the plates (see eq 7), with $\hat{u}$ the unit vector normal to the plate. One reason why rotational diffusion may contribute to the decay of the EACF is due to the dependence of the scattered intensity on particle orientation. Neglecting translation−rotation coupling at this stage, one finds, similar to the derivation for rods as given in ref 15,

$$\hat{g}_E(K,t) = \exp[-DK^2t]\sum_{n=0}^{\infty} S_{2n}(K,d,l)\exp[-D_r n(n+1)t] \tag{24}$$

with

$$S_{2n}(K,d,l) = \frac{4n+1}{2}\frac{\left(\int_{-1}^{1} P_{2n}(x)\, j(d,l,x)\, dx\right)^2}{\int_{-1}^{1} j_0^{\,2}(d,l,x)\, dx} \tag{25}$$

where $x = \cos\theta$, with θ being the angle between $\hat{u}$ and the z-axis, and P_{2n} the second order Legendre polynomial. In Figure 9 numerical results for the S_{2n}-coefficients are shown, represented as a function of Kd since the dependence on l is rather weak ($Kl \ll 1$). For $Kd < 5$, the relative weight of the S_{2n}, $n > 0$ coefficients reflecting rotational contributions turns out to be at most 8% of the purely translational S_0−coefficient.

The second contribution of rotational diffusion to the decay of the EACF stems from the coupling between rotation and translation, due to the difference in friction for translations either parallel or perpendicular to the particle symmetry axis. For short times, the coupling function which appears in eq 10 is equal to

$$C(K,d,l) = \frac{1}{2P(K,d,l)}\int_{-1}^{1} j^2\left(\frac{1}{2}Kxd\right)\left(x^2 - \frac{1}{3}\right) dx \tag{26}$$

The result of numerical evaluation of this integral is shown in Figure 9, plotted as a function of Kd because of the practical independence of the form factor on the thickness l for the K-vectors of the experiment. The subsequent contribution to the decay of the EACF due to rotation−translation coupling can be estimated from eq 10. For plates, for which $|\Delta D| \approx D$ (see eq 2), this contribution is at most 5% at times where $DK^2t = 1$, if $Kd < 5$.

Acknowledgment. This work was supported by the Foundation for Fundamental Research on Matter (FOM) which is part of The Netherlands Organization for the Advancement of Research (NWO).

LA991571B